Origin of slow spontaneous resting-state neuronal fluctuations in brain networks

Giri P. Krishnan[a,1], Oscar C. González[a,b,1], and Maxim Bazhenov[a,b,2]

[a]Department of Medicine, University of California, San Diego, La Jolla, CA 92093; and [b]Neuroscience Graduate Program, University of California, San Diego, La Jolla, CA 92093

Edited by Marcus E. Raichle, Washington University in St. Louis, St. Louis, MO, and approved May 10, 2018 (received for review September 8, 2017)

Resting- or baseline-state low-frequency (0.01–0.2 Hz) brain activity is observed in fMRI, EEG, and local field potential recordings. These fluctuations were found to be correlated across brain regions and are thought to reflect neuronal activity fluctuations between functionally connected areas of the brain. However, the origin of these infra-slow resting-state fluctuations remains unknown. Here, using a detailed computational model of the brain network, we show that spontaneous infra-slow (<0.05 Hz) activity could originate due to the ion concentration dynamics. The computational model implemented dynamics for intra- and extracellular K^+ and Na^+ and intracellular Cl^- ions, Na^+/K^+ exchange pump, and KCC2 cotransporter. In the network model simulating resting awake-like brain state, we observed infra-slow fluctuations in the extracellular K^+ concentration, Na^+/K^+ pump activation, firing rate of neurons, and local field potentials. Holding K^+ concentration constant prevented generation of the infra-slow fluctuations. The amplitude and peak frequency of this activity were modulated by the Na^+/K^+ pump, AMPA/GABA synaptic currents, and glial properties. Further, in a large-scale network with long-range connections based on CoCoMac connectivity data, the infra-slow fluctuations became synchronized among remote clusters similar to the resting-state activity observed in vivo. Overall, our study proposes that ion concentration dynamics mediated by neuronal and glial activity may contribute to the generation of very slow spontaneous fluctuations of brain activity that are reported as the resting-state fluctuations in fMRI and EEG recordings.

resting-state fluctuations | ion concentration dynamics | network models

Resting-state or spontaneous background fluctuations, in the frequency range of 0.01–0.2 Hz (1–16), are reported by a wide range of neuroimaging methods, including electrophysiological, optical, EEG, and fMRI (2, 4, 5, 8, 14, 17). The spontaneous resting-state activity in fMRI signal is a robust phenomenon that has been widely used to evaluate brain network properties, from determining functional connectivity during cognitive tasks to identifying altered functional connectivity in various conscious and disease states (2, 4, 5, 15, 18, 19). The resting-state activity across wide brain regions forms functional networks, such as the default-mode network, that vary with brain state and type of cognitive activity (2, 5, 15, 18). Several neurological and psychiatric disorders, such as epilepsy and schizophrenia, have been shown to correlate with altered resting-state fluctuations and functional connectivity (4, 18–22). Although there is growing interest in understanding the resting-state fluctuations, the underlying neural mechanisms by which these oscillations arise remain unknown.

Previous experimental work showed that infra-slow fluctuations in the local field potential gamma power, neuronal firing rate, and slow cortical potentials exhibit a correlational relationship with the resting-state fMRI blood-oxygen-level-dependent (BOLD) fluctuations (7, 8, 10, 13–15). Further, the underlying structural connectivity of a brain network was shown to shape the functional connectivity estimated from resting-state activity (6, 9, 23, 24). Computational studies suggested the role of intrinsic noise, coupling strengths, conduction velocities, and underlying structural connectivity in the generation of resting-state fluctuations (3, 9, 23). However, these earlier modeling studies used the phenomenological mean field type models and so the underlying biophysical properties giving rise to the infra-slow time scale based on the properties of individual neurons and their networks remain to be understood.

Changes in the ion concentrations have been suggested to modulate network activity (25–34) and extracellular potassium concentrations ($[K^+]_o$) have been shown to fluctuate during resting-state or background activity over a long time period (35). Recordings from anesthetized cat cortex have shown that $[K^+]_o$ may exhibit small-amplitude (~0.5 mM) infra-slow fluctuations around a mean concentration (35). Additionally, $[K^+]_o$ recordings in animal models of epilepsy have shown substantial fluctuations before and during bouts of seizure-like activity (30, 31, 36). A number of computational models suggested a prominent role of potassium concentration dynamics in modulating neuronal excitability and synchrony (25–29, 32, 37). Previous studies have shown that slow spontaneous rhythmic activity in chick spinal cord may arise through accumulation and removal of intracellular chloride (33, 34). Changes in the ionic gradients have been reported to underlie slow bursting dynamics in epilepsy (38, 39). We now know that slow neuronal dynamics can emerge without the presence of the slow time constants in the ion channel dynamics. The central hypothesis of this study is that ion gradient build up and discharge, as well as ion pumping, may result in the infra-slow time scale of the resting-state fluctuations.

Our study predicts that resting-state activity can arise from infra-slow fluctuations of the Na^+ and K^+ ion concentrations. It suggests that the low-amplitude ion concentration dynamics may

Significance

Resting-state infra-slow brain activity fluctuations are observed across various cognitive and disease brain states. Although resting-state fluctuations have received a great deal of interest over the past few years, the underlying biophysical mechanisms are not known. Using computational modeling, we show that spontaneous resting-state fluctuations arise from dynamic ion concentrations and are influenced by the Na^+/K^+ pump, glial K^+ buffering, and AMPA/GABA synaptic currents. These findings provide insights into the biophysical mechanisms underlying generation of this phenomenon and may lead to better understanding of how different cognitive or disease states influence resting-state activity.

Author contributions: G.P.K., O.C.G., and M.B. designed research; G.P.K. and O.C.G. performed research; G.P.K. and O.C.G. analyzed data; and G.P.K., O.C.G., and M.B. wrote the paper.

The authors declare no conflict of interest.

This article is a PNAS Direct Submission.

[1]G.P.K. and O.C.G. contributed equally to this work.

[2]To whom correspondence should be addressed. Email: mbazhenov@ucsd.edu.

This article contains supporting information online at www.pnas.org/lookup/suppl/doi:10.1073/pnas.1715841115/-/DCSupplemental.

Published online June 8, 2018.

allow for local and long-range synchronization among the distant networks. This mechanism can explain correlated and anticorrelated activities between clusters of neurons through long-range synaptic projections, which reflect underlying network structural connectivity in agreement with the experimental observations of the resting-state activity.

Results

The biophysical network model developed in this study incorporated synaptically coupled excitatory pyramidal neurons (PYs) and inhibitory interneurons (INs), both receiving random Poisson drive, and implemented realistic dynamics of the major ion concentrations to provide in vivo-like conditions (26–29, 37). A "single-cluster" network model possessed only local connectivity (five-neuron radius). Below we will first explore dynamics of a single-cluster network and then expand it to the case of several clusters connected with long-range synaptic connections.

In a network consisting of a single cluster of 50 neurons (Fig. 1 *A1*), PY and IN population activity appeared random over a period of 800-s simulation time (Fig. 1 *A2*). However, analysis of the mean firing rate of PYs revealed a very slow semiperiodic fluctuation (Fig. 1*B*). Similar fluctuations were observed in the band-pass-filtered mean PY membrane voltage (Fig. 1*C*), mean extracellular K^+ ($[K^+]_o$) and intracellular Na^+ ($[Na^+]_i$) concentrations (Fig. 1*D* green and red respectively), and mean Na^+/K^+ pump current (Fig. 1*E*). The $[K^+]_o$ fluctuation was 0.1–0.2 mM in amplitude, while the $[Na^+]_i$ fluctuation was about 0.05 mM in amplitude. Power spectrum of the mean $[K^+]_o$, $[Na^+]_i$, Na^+/K^+ pump current, membrane voltage, and network firing rate revealed a peak at around 0.02 Hz (Fig. 1*F*).

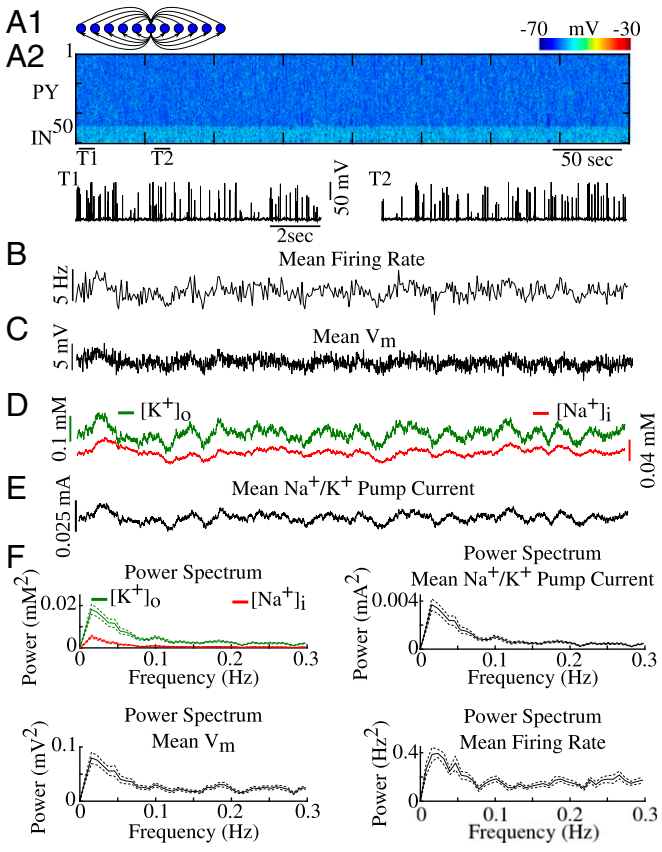

Fig. 1. Minimal cortical network model exhibits resting-state fluctuations. (*A1*) Cartoon of the basic network architecture. (*A2*) Spontaneous activity in the network of PYs and INs. T1 and T2 indicate times expanded below in single PY cell traces. (*B–E*) Mean PY firing rate, mean filtered (0.001–0.1 Hz) membrane voltage, $[K^+]_o$ and $[Na^+]_i$, and Na^+/K^+ pump current dynamics, respectively. (*F*) Power spectrums of the mean PY firing rate, membrane voltage, $[K^+]_o$ and $[Na^+]_i$, and Na^+/K^+ pump current.

Both mean $[K^+]_o$ and $[Na^+]_i$ revealed very slow fluctuations, and therefore we first tested the role of these ions in the generation of the resting-state activity in our network model. Holding the K^+ concentration constant resulted in a loss of the infra-slow oscillatory activity in the mean membrane voltage of the PYs, regardless of the specific values of the concentration (Fig. 2*A*, *Top*, red). Power spectrum analysis revealed disappearance of a low-frequency peak and almost flat spectrum (Fig. 2*B*, *Inset*). In contrast, preventing the Na^+ fluctuation did not result in a loss of the infra-slow membrane voltage fluctuations (Fig. 2 *A* and *B*, *Right*). This suggests that fluctuations of K^+ play a major role in the generation of the resting-state activity, while Na^+ fluctuation may play a modulatory role.

We next explored the role the Na^+/K^+ pump current, glia K^+ buffering, AMPA/GABA synaptic connections, and ion diffusion in the properties of the resting-state fluctuations. Increasing the strength of the Na^+/K^+ pump resulted in decreased fluctuation amplitude of the pump current as revealed by the reduced peak in the power spectrum (Fig. 2*C*, black) and increase in the peak frequency (Fig. 2*C*, red). For higher strength of the Na^+/K^+ pump, the relative changes of the extracellular K^+ were reduced, leading to the smaller resting-state fluctuations. Similarly, decreasing the half activation concentration of $[K^+]_o$ in glia cells, that increased effectiveness of glia buffering, reduced the resting-state fluctuation amplitude (Fig. 2*D*). Thus, the slow dynamic processes controlling accumulation of the ions and their removal determined the amplitude and the peak frequency of the slow fluctuations. Further, increasing the strength of the AMPA connections between PYs increased the amplitude of the resting-state fluctuations while shifting peak frequency to the lower values (Fig. 2*E*). GABA, however, had minimal impact on the amplitude of the resting-state fluctuations but shifted the peak frequency to the higher values (Fig. 2*E*). Increase in the fluctuation amplitude due to increase in the AMPA connection strength suggests that recurrent synaptic excitation promoted faster and higher-level buildup of the extracellular K^+ concentration, thus leading to stronger and faster resting-state fluctuations. Diffusion of ions in the extracellular space was not required for the infra-slow activity (Fig. S5) and the infra-slow fluctuations in this model did not depend on the random number generation protocol that was used for Poisson stimulation (Fig. S4).

To explore the mechanisms behind the infra-slow activity, we analyzed the ion concentration dynamics near the positive and negative peaks of the mean firing rate (Fig. S1). We found that the ion concentrations and firing rate were reduced (elevated) for up to 20 s before the positive (negative) firing rate peaks (Fig. S1 *E* and *F*). It suggests that the observed infra-slow activity may raise from the combination of the positive and negative feedback interactions between $[K^+]_o/[Na^+]_i$ and neuronal excitability, which depend on the absolute level of the ion concentrations (28). This proposed mechanism was further confirmed by the existence of slow oscillations in a simplified network model with dc input instead of stochastic Poisson drive (Fig. S3). To estimate the time scale of the ion concentration dynamics in the model, we examined the amplitude and duration of the transient events following small changes in external input (Fig. S2) and we found large transients of the firing rate and the ion concentrations lasting ~20 s (Fig. S2 *A–C*).

Does the network size affect generation of the resting-state activity? To answer this question, we increased the number of neurons in the network to 500. The network included only local connections (i.e., five-neuron radius). We found that the amplitude of the infra-slow fluctuations obtained from the averaged activity of the entire 500-neuron network was smaller than in our control 100-neuron network. To understand this phenomenon,

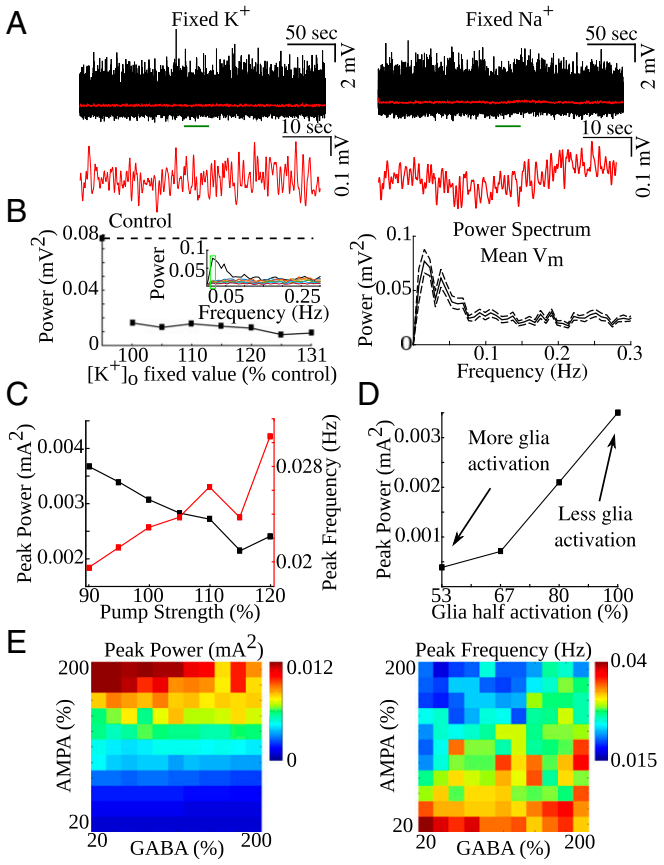

Fig. 2. Ion concentrations, Na^+/K^+ pump, glial K^+ buffering, and AMPA/GABA strength influence properties of the resting-state fluctuations. (*A*) Mean membrane voltages (black) and mean filtered membrane voltages (red) for the networks with either fixed K^+ (*Left*) or fixed Na^+ (*Right*). (*B*, *Left*) Power spectrum peak power as a function of fixed K^+ concentration. Percentage is based on the mean $[K^+]_o$ in control network. Dotted black line shows peak power in control network. (*Inset*) Individual power spectrums for different fixed K^+ conditions. Black line shows a control condition. Green box indicates the region used to compute peak power. (*B*, *Right*) Corresponding power spectrum of the mean membrane voltage in fixed Na^+ condition in *A*. (*C*) Peak power (black) and peak frequency (red) as a function of Na^+/K^+ pump current strength. (*D*) Power spectrum peak power as a function of glia model half activation K^+ concentration. (*E*) Power spectrum peak power as a function of AMPA and GABA connection strengths (*Left*). Power spectrum peak frequency as a function of AMPA and GABA connection strengths (*Right*).

we examined independently activity in the smaller subsets of neurons (100-neuron subsets from the 500-neuron network) (Fig. 3 *A* and *B*). We observed in each such subnetwork fluctuations of the same amplitude as in the control 100-neuron network. When random long-range connectivity was introduced within the 500-neuron network, we observed an increase of spontaneous fluctuations. This suggests that local synaptic connections and ion diffusion were sufficient to synchronize the smaller network but not the larger one. In the latter case, the network activity broke into semiindependent clusters, where each cluster could oscillate out of phase with the other clusters. Long-range connections synchronized distinct clusters. This was also further confirmed by a large-scale simulation using CoCoMac connectivity.

Structures comprising functional networks, such as the ventromedial prefrontal cortex and posterior cingulate cortex of the default mode network, have been shown to display coherent resting-state fluctuations (5). Although fluctuations of the local ion concentrations, as proposed by our study, may underlie intrinsic fluctuations in these regions, the spatial separation of these regions makes sharing of the extracellular space between them unlikely. Therefore, these distinct regions should have independent dynamics of the local ion concentrations. However, many brain regions are known to be connected through long-range synaptic projections. Thus, we next tested whether our model could also generate coherent fluctuations between distinct clusters of neurons connected through long-range synaptic connections where each cluster had local synaptic connectivity and local extracellular ion concentration dynamics (Fig. 4). We kept the same connectivity scheme (Fig. 1 *A1*) within each neuron cluster but prevented ions from diffusing between the two clusters. Additionally, we added long-range sparse synaptic projections between the two clusters through excitatory PY–PY connections. While spiking activity in either cluster appeared to be random (Fig. 4 *A2*), the mean Na^+/K^+ pump current within each cluster revealed synchronized resting-state fluctuations (Fig. 4*B*) that peak around 0.02 Hz (Fig. 4*C*, *Left*). Importantly, fluctuations of the mean membrane potential and mean Na^+/K^+ current in both clusters revealed positive cross-correlation (Fig. 4*C*, *Middle* and *Right*, respectively).

We next varied the AMPA connection strength of the long-range connections between the two clusters and we computed

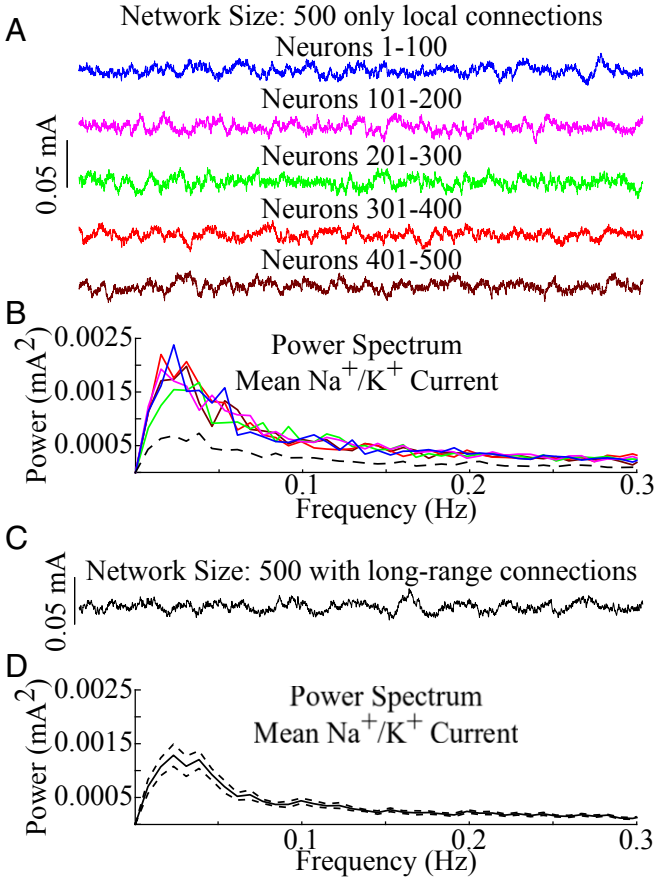

Fig. 3. Effects of network size on the resting-state fluctuation amplitude. (*A*) Mean Na^+/K^+ pump currents from clusters of 100 neurons comprising the network of 500 neurons with only local connections. Note the lack of synchronization between individual clusters. (*B*) Power spectrums calculated from the mean Na^+/K^+ pump currents in the individual clusters (colored lines match colors in *A*), and power spectrum of the averaged Na^+/K^+ pump current from the entire 500-neuron network (dashed line). (*C*) Mean Na^+/K^+ pump current from the network of 500 neurons implementing both local and long-range connections. (*D*) Power spectrum of Na^+/K^+ pump current from the network in *C*. Dashed lines represent SEM.

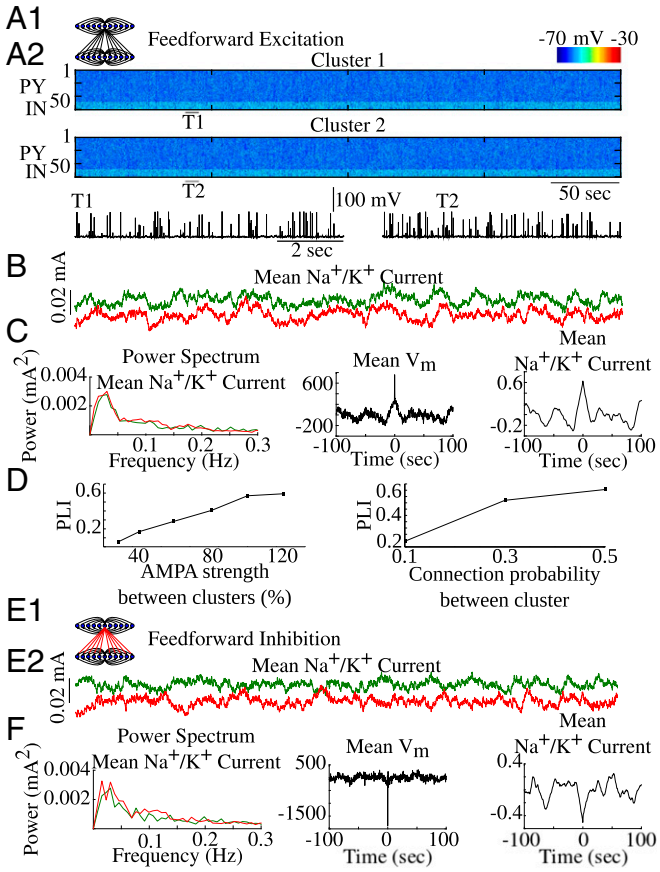

Fig. 4. Long-range connections synchronize resting-state fluctuations. (*A1*) Cartoon of the network model with feedforward excitation. (*A2*) Spontaneous activity in the neuronal clusters connected by feedforward excitation. T1 and T2 indicate times expanded below in single PY traces. (*B*) Mean Na^+/K^+ pump currents for each cluster in *A*. (*C*) Power spectrums of the Na^+/K^+ pump currents in *B* (*Left*), cross-correlation of the mean filtered membrane potentials from clusters in *A* (*Middle*), and cross-correlation of the mean Na^+/K^+ pump currents from *B* (*Right*). (*D*) PLI as a function of feedforward AMPA strength (*Left*) and connection probability (*Right*). (*E1*) Cartoon of the network model with feedforward inhibition. (*E2*) Mean Na^+/K^+ pump currents for each cluster connected through feedforward inhibition. (*F*) Power spectrums of Na^+/K^+ pump currents in *E2* (*Left*), cross-correlation of the mean filtered membrane potentials from clusters with feedforward inhibition (*Middle*), and cross-correlation of the mean Na^+/K^+ pump currents from *E2* (*Right*).

the phase-locking index (PLI) between the mean Na^+/K^+ pump currents of the two clusters for different AMPA strengths. Increasing the strength of the long-range connections (Fig. 4*D*, *Left*) or connection probability (Fig. 4*D*, *Right*) resulted in higher phase locking between the signals. Importantly, even for relatively low connection strength and probability, the PLI remained significantly higher than that for two disconnected clusters, which oscillated fully independently (Fig. S6).

To test if the model can explain anticorrelated resting-state fluctuations observed in vivo (40–42), we increased the strength of the AMPA connection between excitatory PYs of one cluster and inhibitory INs of another cluster and observed negatively correlated resting-state fluctuations (Fig. 4 *E1*, *E2*, and *F*). Altogether, these findings suggest that the mechanisms proposed in our model can account for resting-state fluctuations in local regions as well as for positively and negatively correlated fluctuations between distinct brain regions.

Finally, to test whether our model could explain in vivo data that revealed correlations between structural and functional connectivity in the macaque brain (6, 9, 23, 24), we modeled 58 different brain regions of the macaque brain using connectivity information gathered from the CoCoMac structural connectivity database (cocomac.g-node.org/main/index.php?). Each of the 58 regions was modeled as a cluster of 50 excitatory PYs and 10 inhibitory INs with connectivity within a cluster identical to that shown in Fig. 1 *A1*. Long-range excitatory PY–PY connections were formed between clusters based on the CoCoMac structural connectivity data set (cocomac.g-node.org/main/index.php?). We computed the correlation coefficient between Na^+/K^+ pump currents in different clusters for every possible pair of clusters. This analysis revealed the groups of clusters that showed a high degree of correlation (Fig. 5*A*, *Middle*). To quantify the relationship between structural and functional connectivity, we next computed the correlation coefficient between clusters (brain regions) showing significant correlation of the mean Na^+/K^+ pump currents (Fig. 5*A*, *Middle*) and the clusters with strong structural connectivity (Fig. 5*A*, *Left*). We found a significant correlation between the functional and structural connectivity ($r = 0.20508$) (Fig. 5*A*, *Right*). Thus, we concluded that a network with local (cluster specific) ion concentration dynamics and long-range

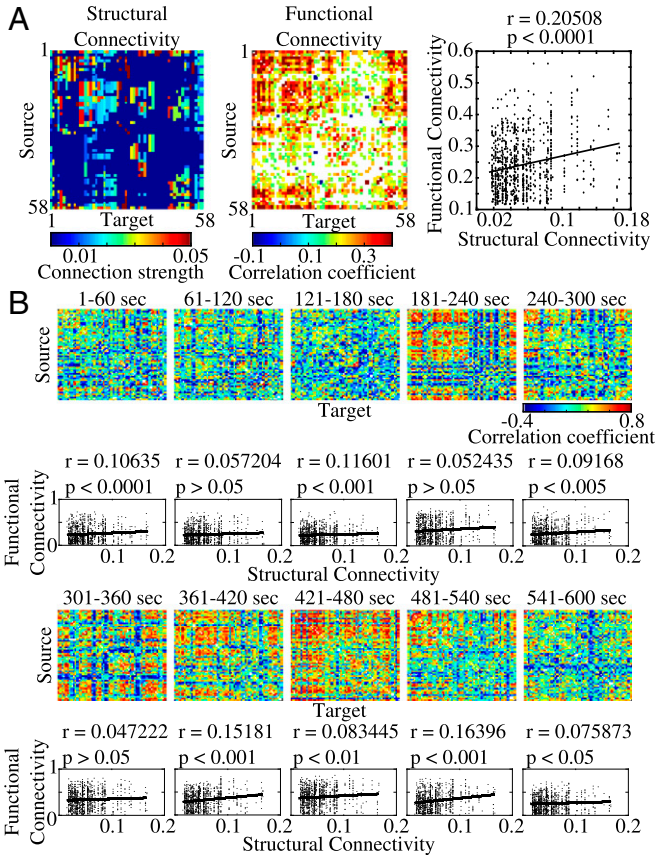

Fig. 5. Macaque simulations. (*A*, *Left*) Structural connectivity matrix for macaque network from the CoCoMac structural connectivity database (cocomac.g-node.org/main/index.php?). (*A*, *Middle*) Functional connectivity calculated from the network model including 58 individual network clusters. Only significant correlations are shown (Bonferroni corrected for multiple comparisons). (*A*, *Right*) Correlation of functional and structural connectivity. (*B*) Heat maps show functional connectivity computed for consecutive 60-s time windows demonstrating the dynamic nature of the functional connectivity in the network model. Color indicates the correlation between infra-slow fluctuations in the simulated brain regions. Bottom plots show correlations between functional connectivity computed in the corresponding heat map and structural connectivity in *A*. Correlation coefficient and *P* values are reported for comparison between the functional connectivity computed during each time bin and the structural connectivity in *A*.

synaptic connectivity between clusters can account for the experimentally observed relationship between structural and functional connectivity.

Recent data revealed the dynamic nature of functional connectivity (43–46). It has been shown that the strength of the functional connectivity computed from the resting-state fluctuations between regions comprising the default mode network can vary in time (1). To check for a similar characteristic in our model, we computed the correlation coefficients for 10 subsequent 60-s bins (Fig. 5*B*). Similar to experimental findings, our model revealed dynamic changes of the functional connectivity (Fig. 5*B*). The network exhibited both instances of strong and weak functional connectivity between specific clusters for different time epochs. Interestingly, the regions that showed mostly weak functional connectivity could develop strong connectivity transiently in time before returning to a low-connectivity state.

Discussion

In this study we tested the hypothesis that dynamics of the ion concentrations, regulated through the neuronal and glial activity, may form the basis of the resting-state fluctuations in the brain. Comprising only about 2% of the total body weight of an average adult human, the brain is responsible for up to 20% of the total energy consumption (16). Task-evoked responses generally increase brain energy consumption by less than 5% (47). Although so much energy is consumed to maintain a baseline level of activity, little is known about its use, including spontaneous resting-state fluctuations in the brain. It was first observed by Biswal et al. (17) that the spontaneous background fluctuations recorded during fMRI scans were coherent between functionally related brain regions. Since then, other studies have shown similar coherent resting-state activity between regions comprising functional networks such as the default mode network and executive control network (2, 4–6, 11, 16, 47). Interestingly, infra-slow (<0.2 Hz) resting-state fluctuations have been observed in various cognitive states (2, 5, 11, 15) and can exhibit modified temporal coherence patterns in various neurological and psychiatric conditions (4, 18, 19). In our study we proposed and tested the hypothesis that resting-state fluctuations may depend on the ion concentration dynamics, specifically $[K^+]_o$ fluctuations, and that the phase coherence of the infra-slow activities between distinct brain regions depends on the long-range synaptic connectivity. Our model based on the CoCoMac structural connectivity database explained the relationship between structural and functional connectivity that was revealed in studies of resting-state activity in the macaque brain.

The characteristic time scale of the resting-state fluctuations is of the order of 50–100 s. Very few neural processes are known to act at such a slow time scale. Here we report that the ion concentrations may spontaneously vary with a very slow time scale and could act as the modulator of the neural activity leading to emergence of resting-state fluctuations. Increase of the $[K^+]_o$ results in higher excitability of neurons which may then trigger further elevation of the extracellular K^+, leading to the positive feedback loop (26–28, 37). Importantly, increase of $[K^+]_o$ can be arbitrarily slow, being determined by the balance of the inward and outward K^+ flux. Increase in the $[Na^+]_i$ terminates the positive feedback loop (28) initiating a phase of progressive decrease of the ion concentrations and firing rate. Transitions between these phases depend on the Na^+/K^+ pump that becomes significantly more activated as the K^+ and Na^+ reach critical values; this leads to the changes of the outward pump current that affects intrinsic excitability. Indeed, experimental data suggest that the ion concentrations may have slow dynamics similar to the time course of the resting-state fluctuations (25–27, 30–36, 48). Our previous studies revealed that the ion concentration dynamics may lead to the slow (<0.2 Hz) quasi-periodic transitions between distinct network states (bursting and tonic firing) (25–28, 30–32, 35, 36, 48, 49). Other studies have suggested the role of slow processes involving ion dynamics and Na^+/K^+ pump activity in information processing (50, 51).

The gradual accumulation of $[K^+]_o$ has been shown to contribute to development of seizure-like discharges (26–28, 32, 37). Studies in patients with epilepsy revealed abnormal resting-state fluctuations (18, 20, 21). Indeed, it has been demonstrated that the amplitude of resting-state fluctuations in epileptic patients is increased compared with the healthy individuals (20). Interestingly, our previous work demonstrated that homeostatic up-regulation of excitatory connections, following trauma, may lead to rewiring long-range cortical connectivity and promote spontaneous seizures, along with relatively high amplitude very slow baseline fluctuations (37). Taken together, these results may explain differences in the resting-state fluctuation properties in epileptic patients and healthy individuals.

Studies in animals revealed a correlation between anatomical structural and functional connectivity (6, 9, 23, 24). It was proposed with computer models that the time scale of infra-slow fluctuations could be a result of transient bouts of synchrony between clusters of nodes, and that the functional connectivity arising in the network strongly reflected the underlying structural architecture (9, 23). Phase locking between distant network sites through long-range connections was reported in the mean-field-type models (3, 6, 9). However, phase locking of the infra-slow activity in the network models implementing biophysical mechanisms of oscillation and sparse long-range connections, as described in our study, has not been previously reported. In agreement with previous data (9, 23), functional connectivity in our model, computed over a long time window, reliably reflected the underlying structural connectivity.

Lack of monosynaptic connections between brain regions does not accurately predict the absence of the functional connectivity between those regions (5). However, coupling strength between neuronal clusters has been suggested to influence the strength of correlated and anticorrelated activity between nodes (23). We found that the balance of long-range feedforward projections to excitatory PYs vs. inhibitory INs of remote cluster determines the phase-locking mode—correlated or anticorrelated fluctuations—and we observed dynamic changes of the functional connectivity over time, in agreement with the experimental studies (43–46).

Resting-state infra-slow fluctuations were originally observed during baseline recordings of the BOLD signals in fMRI studies (7, 16, 22, 47). Changes in oxygen consumption, a result of reestablishing ion gradients through active pumping following increases in activity, give rise to fluctuations in BOLD signals (4, 5, 7, 42). Through oxidative phosphorylation, oxygen allows for the production of ATP, thereby providing the cells with energy necessary to, among other processes, reestablish ionic gradients through ion pumping (52). As such, the production of ATP is limited by the time scale of oxygen consumption and the replenishing of oxygen/glucose reservoirs (52, 53). The flux in glucose/oxygen consumption and neurovascular coupling have been suggested to occur on a slow time scale, leading to the slow network dynamics (32, 52–54). Our model does not explore the neurovascular coupling but instead focuses on the mechanisms arising from the interaction between neuronal and ion concentration dynamics. It suggests that taking into account effects of the ion concentrations and Na^+/K^+ pump dynamics may be necessary to capture the biophysical mechanisms leading to generation of infra-slow fluctuations in fMRI recordings. Future work exploring the interaction between neuronal and vascular dynamics is needed to advance our understanding of the complex mosaic of the biophysical mechanisms underlying the BOLD signal and may provide insights into how altered brain and disease states influence resting-state oscillations.

Materials and Methods

Computational Model. The network model implemented dynamics of the ion concentrations as described in detail elsewhere (25, 26, 28, 37). The network consisted of excitatory PYs and inhibitory INs with a 5:1 ratio. Both neuron types were modeled as two-compartmental conductance-base neurons with axosomatic and dendritic compartments. Ion concentration dynamics were implemented for intracellular and extracellular K^+ and Na^+ and intracellular Cl^- and Ca^{2+}. Na^+/K^+ pump Na^+ and K^+ regulation and KCC2 cotransporter Cl^- extrusion were included in both neuron types. Glial regulation of extracellular K^+ was modeled as a free buffer as described in our previous work (28, 29, 37). All neurons received random Poisson drive.

Excitatory synaptic connections were mediated through AMPA and NMDA conductances and inhibitory synaptic connections were mediated through $GABA_A$. Local connectivity (within a single cluster) was restricted to a radius of five neurons for PY–PY connections. Long-range connections between clusters (i.e., feedforward excitation or inhibition) were mediated by AMPA and NMDA conductances between PYs from one cluster to PYs (feedforward excitation) or INs (feedforward inhibition) of a second cluster with a 25% connection probability. For macaque simulations, 58 brain regions were modeled as independent clusters of neurons with long-range connections between clusters based on structural connectivity data from the CoCoMac database (cocomac.g-node.org/main/index.php?). Functional connectivity was computed as the correlation coefficients between mean Na^+/K^+ pump currents from the individual clusters. More detailed description of the model is provided in *SI Materials and Methods*.

Data Availability. Code for our network model, analysis scripts, and simulation data are available at https://www.bazhlab.ucsd.edu/.

ACKNOWLEDGMENTS. This study was supported by Office of Naval Research Multidisciplinary University Research Initiative Grant N000141612829 and NSF Graduate Research Fellowship Grant DGE-1326120 (to O.C.G.).

1. Chang C, Glover GH (2010) Time-frequency dynamics of resting-state brain connectivity measured with fMRI. *Neuroimage* 50:81–98.
2. Fukunaga M, et al. (2006) Large-amplitude, spatially correlated fluctuations in BOLD fMRI signals during extended rest and early sleep stages. *Magn Reson Imaging* 24: 979–992.
3. Ghosh A, Rho Y, McIntosh AR, Kötter R, Jirsa VK (2008) Noise during rest enables the exploration of the brain's dynamic repertoire. *PLOS Comput Biol* 4:e1000196.
4. Greicius M (2008) Resting-state functional connectivity in neuropsychiatric disorders. *Curr Opin Neurol* 21:424–430.
5. Greicius MD, et al. (2008) Persistent default-mode network connectivity during light sedation. *Hum Brain Mapp* 29:839–847.
6. Greicius MD, Supekar K, Menon V, Dougherty RF (2009) Resting-state functional connectivity reflects structural connectivity in the default mode network. *Cereb Cortex* 19:72–78.
7. He BJ, Snyder AZ, Zempel JM, Smyth MD, Raichle ME (2008) Electrophysiological correlates of the brain's intrinsic large-scale functional architecture. *Proc Natl Acad Sci USA* 105:16039–16044.
8. Hiltunen T, et al. (2014) Infra-slow EEG fluctuations are correlated with resting-state network dynamics in fMRI. *J Neurosci* 34:356–362.
9. Honey CJ, Kötter R, Breakspear M, Sporns O (2007) Network structure of cerebral cortex shapes functional connectivity on multiple time scales. *Proc Natl Acad Sci USA* 104:10240–10245.
10. Khader P, Schicke T, Röder B, Rösler F (2008) On the relationship between slow cortical potentials and BOLD signal changes in humans. *Int J Psychophysiol* 67:252–261.
11. Larson-Prior LJ, et al. (2009) Cortical network functional connectivity in the descent to sleep. *Proc Natl Acad Sci USA* 106:4489–4494.
12. Lörincz ML, Geall F, Bao Y, Crunelli V, Hughes SW (2009) ATP-dependent infra-slow (<0.1 Hz) oscillations in thalamic networks. *PLoS One* 4:e4447.
13. Palva JM, Palva S (2012) Infra-slow fluctuations in electrophysiological recordings, blood-oxygenation-level-dependent signals, and psychophysical time series. *Neuroimage* 62:2201–2211.
14. Pan WJ, Thompson GJ, Magnuson ME, Jaeger D, Keilholz S (2013) Infraslow LFP correlates to resting-state fMRI BOLD signals. *Neuroimage* 74:288–297.
15. Picchioni D, et al. (2011) Infraslow EEG oscillations organize large-scale cortical-subcortical interactions during sleep: A combined EEG/fMRI study. *Brain Res* 1374:63–72.
16. Raichle ME (2015) The restless brain: How intrinsic activity organizes brain function. *Philos Trans R Soc Lond B Biol Sci* 370:20140172.
17. Biswal B, Yetkin FZ, Haughton VM, Hyde JS (1995) Functional connectivity in the motor cortex of resting human brain using echo-planar MRI. *Magn Reson Med* 34: 537–541.
18. Vanhatalo S, et al. (2004) Infraslow oscillations modulate excitability and interictal epileptic activity in the human cortex during sleep. *Proc Natl Acad Sci USA* 101: 5053–5057.
19. Zhang D, Raichle ME (2010) Disease and the brain's dark energy. *Nat Rev Neurol* 6: 15–28.
20. Gupta L, et al. (2017) Towards prognostic biomarkers from BOLD fluctuations to differentiate a first epileptic seizure from new-onset epilepsy. *Epilepsia* 58:476–483.
21. Lui S, et al. (2008) Differential interictal activity of the precuneus/posterior cingulate cortex revealed by resting state functional MRI at 3T in generalized vs. partial seizure. *J Magn Reson Imaging* 27:1214–1220.
22. Raichle ME (2010) Two views of brain function. *Trends Cogn Sci* 14:180–190.
23. Deco G, Jirsa V, McIntosh AR, Sporns O, Kötter R (2009) Key role of coupling, delay, and noise in resting brain fluctuations. *Proc Natl Acad Sci USA* 106:10302–10307.
24. Deco G, Jirsa VK, McIntosh AR (2011) Emerging concepts for the dynamical organization of resting-state activity in the brain. *Nat Rev Neurosci* 12:43–56.
25. Bazhenov M, Timofeev I, Steriade M, Sejnowski TJ (2004) Potassium model for slow (2-3 Hz) in vivo neocortical paroxysmal oscillations. *J Neurophysiol* 92:1116–1132.
26. Fröhlich F, Bazhenov M (2006) Coexistence of tonic firing and bursting in cortical neurons. *Phys Rev E Stat Nonlin Soft Matter Phys* 74:031922.
27. Fröhlich F, Bazhenov M, Iragui-Madoz V, Sejnowski TJ (2008) Potassium dynamics in the epileptic cortex: New insights on an old topic. *Neuroscientist* 14:422–433.
28. Krishnan GP, Bazhenov M (2011) Ionic dynamics mediate spontaneous termination of seizures and postictal depression state. *J Neurosci* 31:8870–8882.
29. Krishnan GP, Filatov G, Shilnikov A, Bazhenov M (2015) Electrogenic properties of the Na^+/K^+ ATPase control transitions between normal and pathological brain states. *J Neurophysiol* 113:3356–3374.
30. Pedley TA, Fisher RS, Moody WJ, Futamachi KJ, Prince DA (1974) Extracellular potassium activity during epileptogenesis: A comparison between neocortex and hippocampus. *Trans Am Neurol Assoc* 99:41–45.
31. Somjen GG (2002) Ion regulation in the brain: Implications for pathophysiology. *Neuroscientist* 8:254–267.
32. Wei Y, Ullah G, Schiff SJ (2014) Unification of neuronal spikes, seizures, and spreading depression. *J Neurosci* 34:11733–11743.
33. Chub N, Mentis GZ, O'donovan MJ (2006) Chloride-sensitive MEQ fluorescence in chick embryo motoneurons following manipulations of chloride and during spontaneous network activity. *J Neurophysiol* 95:323–330.
34. Chub N, O'Donovan MJ (2001) Post-episode depression of GABAergic transmission in spinal neurons of the chick embryo. *J Neurophysiol* 85:2166–2176.
35. McCreery DB, Agnew WF (1983) Changes in extracellular potassium and calcium concentration and neural activity during prolonged electrical stimulation of the cat cerebral cortex at defined charge densities. *Exp Neurol* 79:371–396.
36. Traynelis SF, Dingledine R (1988) Potassium-induced spontaneous electrographic seizures in the rat hippocampal slice. *J Neurophysiol* 59:259–276.
37. González OC, et al. (2015) Modeling of age-dependent epileptogenesis by differential homeostatic synaptic scaling. *J Neurosci* 35:13448–13462.
38. Žiburkus J, Cressman JR, Schiff SJ (2013) Seizures as imbalanced up states: Excitatory and inhibitory conductances during seizure-like events. *J Neurophysiol* 109: 1296–1306.
39. Huberfeld G, Blauwblomme T, Miles R (2015) Hippocampus and epilepsy: Findings from human tissues. *Rev Neurol (Paris)* 171:236–251.
40. Keller JB, et al. (2015) Resting-state anticorrelations between medial and lateral prefrontal cortex: Association with working memory, aging, and individual differences. *Cortex* 64:271–280.
41. Tian L, et al. (2007) The relationship within and between the extrinsic and intrinsic systems indicated by resting state correlational patterns of sensory cortices. *Neuroimage* 36:684–690.
42. Greicius MD, Krasnow B, Reiss AL, Menon V (2003) Functional connectivity in the resting brain: A network analysis of the default mode hypothesis. *Proc Natl Acad Sci USA* 100:253–258.
43. Hutchison RM, et al. (2013) Dynamic functional connectivity: Promise, issues, and interpretations. *Neuroimage* 80:360–378.
44. Hutchison RM, Womelsdorf T, Gati JS, Everling S, Menon RS (2013) Resting-state networks show dynamic functional connectivity in awake humans and anesthetized macaques. *Hum Brain Mapp* 34:2154–2177.
45. Shen K, Hutchison RM, Bezgin G, Everling S, McIntosh AR (2015) Network structure shapes spontaneous functional connectivity dynamics. *J Neurosci* 35:5579–5588.
46. Allen EA, et al. (2014) Tracking whole-brain connectivity dynamics in the resting state. *Cereb Cortex* 24:663–676.
47. Raichle ME, Mintun MA (2006) Brain work and brain imaging. *Annu Rev Neurosci* 29: 449–476.
48. Moody WJ, Futamachi KJ, Prince DA (1974) Extracellular potassium activity during epileptogenesis. *Exp Neurol* 42:248–263.
49. Fröhlich F, Bazhenov M, Timofeev I, Steriade M, Sejnowski TJ (2006) Slow state transitions of sustained neural oscillations by activity-dependent modulation of intrinsic excitability. *J Neurosci* 26:6153–6162.
50. Forrest MD (2014) The sodium-potassium pump is an information processing element in brain computation. *Front Physiol* 5:472.
51. Arganda S, Guantes R, de Polavieja GG (2007) Sodium pumps adapt spike bursting to stimulus statistics. *Nat Neurosci* 10:1467–1473.
52. Wei Y, Ullah G, Ingram J, Schiff SJ (2014) Oxygen and seizure dynamics: II. Computational modeling. *J Neurophysiol* 112:213–223.
53. Ingram J, et al. (2014) Oxygen and seizure dynamics: I. Experiments. *J Neurophysiol* 112:205–212.
54. Longden TA, et al. (2017) Capillary K^+-sensing initiates retrograde hyperpolarization to increase local cerebral blood flow. *Nat Neurosci* 20:717–726.